Chemical Physics Letters 501 (2011) 437–441

Contents lists available at ScienceDirect

Chemical Physics Letters

journal homepage: www.elsevier.com/locate/cplett

Investigation of surface and non-local screening effects in the Ni 2*p* core level photoemission spectra of NiO

R.J.O. Mossanek [a], I. Preda [b], M. Abbate [a], J. Rubio-Zuazo [c], G.R. Castro [c], A. Vollmer [d], A. Gutiérrez [b], L. Soriano [b,*]

[a] Departamento de Física, Universidade Federal do Paraná, Caixa Postal 19044, 81531-990 Curitiba, PR, Brazil
[b] Departamento de Física Aplicada and Instituto de Ciencia de Materiales Nicolás Cabrera, Universidad Autónoma de Madrid, Cantoblanco, 28049 Madrid, Spain
[c] SpLine, European Synchrotron Radiation Facility, Grenoble F-38043, France
[d] Helmholtz Zentrum Berlin fuer Materialien und Energie GmbH, BESSY II, Berlin, Germany

ARTICLE INFO

Article history:
Received 18 July 2010
In final form 16 November 2010
Available online 18 November 2010

ABSTRACT

We studied the Ni 2*p* core-level spectra of NiO using cluster model calculations and X-ray photoemission spectra. The calculations were performed for a NiO_6, a NiO_5, and a NiO_6:NiO_5 cluster, which allows studying the bulk, the surface, and the non-local effects in the spectra. The photoemission spectra were taken with soft (or hard) X-rays to enhance the surface (or bulk) contribution. The calculation shows that both surface and non-local-effects contribute to the shoulder in the experimental data. The photoemission spectra show that the relative intensity of the surface contribution decreases for Hard X-rays.

1. Introduction

The electronic structure of the highly correlated NiO oxide has been controversial for many years. In particular, the origin of some structures in the Ni 2*p* photoemission spectra is still under discussion. The ground state of NiO can be described as a mixture of the $3d^8$, $3d^9\underline{L}$, and $3d^{10}\underline{L}^2$ configurations (where $\underline{L}$ denotes a hole in the ligand band) [1–3]. The Ni 2*p* photoemission spectra (see Figure 1) is formed by the main line ($\underline{c}3d^9\underline{L}$), a charge-transfer satellite ($\underline{c}3d^8$ and $\underline{c}3d^{10}\underline{L}^2$), and a shoulder separated by 1.5 eV from the main line (where $\underline{c}$ stands for a hole in the Ni 2*p* core level). While the assignment of the main peak and the satellite is well established, the interpretation of the shoulder in the spectra is still under discussion.

The shoulder was initially attributed to the chemical shift of Ni^{3+} species present at the NiO surface [4,5]. The shoulder was also assigned to multiplet splitting effects within the $\underline{c}3d^{10}\underline{L}^2$ final state configurations [6]. Later on, Van Veenendaal et al. proposed that the shoulder corresponds to non-local screening effects [7]. Recently, we showed using Ni 2*p* XPS spectra that the shoulder has an important surface component [8]. This conclusion was supported by cluster model calculations in pyramidal symmetry (NiO_5). But the experimental intensity of the shoulder was much higher than that expected from a single surface monolayer [8]. Finally, Taguchi et al. [9] explained the Ni 2*p* spectra of NiO in terms of Zhang-Rice (ZR) doublet bound states.

The most accepted interpretation is that the shoulder comes mostly from non-local screening effects. This explains, for instance, the absence of the shoulder in compounds without Ni neighbors, like $Ni_{0.1}Mg_{0.9}O$ [10]. It also seems consistent with the Ni 2*p* XPS spectra of a NiO monolayer epitaxially grown on MgO [11]. However, this model does not explain the absence of the non-local screening peak in La_2NiO_4 [12]. Further, this model does not explain the increase of the shoulder in the spectra of NiO taken at grazing take-off angles [8]. Therefore, the non-local screening model is not able to address all the questions about the Ni 2*p* photoemission spectra.

In this letter, we performed calculations in NiO_6, NiO_5, and NiO_6:NiO_5 clusters, which allow studying bulk, surface and non-local effects, respectively. We show below that both surface and non-local effects contribute to the intensity of the shoulder. These results are corroborated by the energy dependence of the experimental Ni 2*p* photoemission spectra. In particular, the surface contribution to the shoulder in the spectra decreases for harder X-rays.

2. Experimental details

We studied the core level photoemission spectra of two NiO samples: one was a freshly cleaved NiO (100) single crystal for hard X-ray measurements, and the other a stoichiometric NiO thin film for soft X-ray measurements [13,14]. The measurements were performed at two different synchrotron radiation facilities and in our laboratory. The hard X-ray photoelectron spectrum (HAXPES) taken at 9 keV was measured at the BM25 beamline (Spline) at the ESRF [15] in Grenoble, France. This beamline is equipped with

* Corresponding author. Fax: +34 914973969.
E-mail address: l.soriano@uam.es (L. Soriano).

0009-2614/$ - see front matter © 2010 Elsevier B.V. All rights reserved.
doi:10.1016/j.cplett.2010.11.050

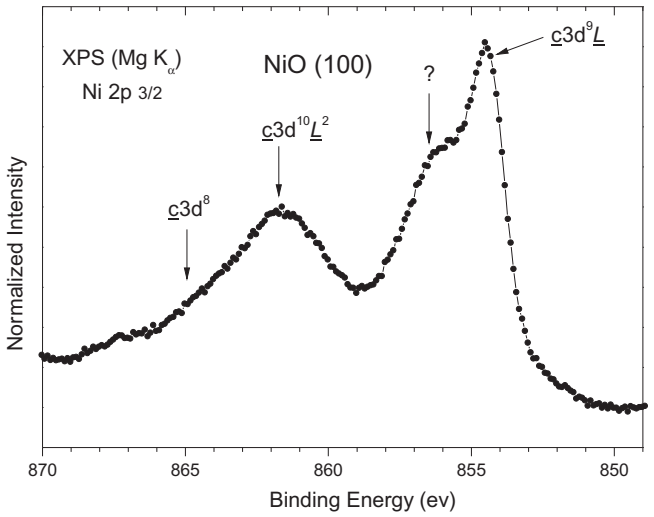

Figure 1. Experimental Ni $2p_{3/2}$ core-level spectra of a NiO (100) single crystal taken with a Mg K_α X-ray source ($h\nu$ = 1253.6 eV).

a double crystal monochromator and a cylindrical sector electron analyzer (CSA300HV) [16,17] developed in cooperation with the Focus GmbH company. This instrument, together with the high brilliance of the BM25 beamline, fulfils the technical requirements imposed by HAXPES. The overall energy resolution for the experiment was about 2.0 eV. The soft X-ray photoemission spectrum (PES) taken at 1.0 keV (PES) was measured at the PM-4 beamline at BESSY, Berlin, Germany. This beamline is equipped with a plane grating monochromator. The spectra were measured by using a Phoybos hemispherical electron energy analyzer. The overall resolution (beamline plus analyzer) was estimated about 0.8 eV. The conventional X-ray photoelectron spectrum (XPS) (1.253 keV) was measured using a CLAM-4 electron energy analyzer working at 20 eV pass energy and giving an overall (X-rays plus analyzer) resolution of about 0.9 eV.

3. Calculation details

The cluster model calculations were performed using two connected NiO_6:NiO_5 clusters. The NiO_6 octahedral cluster accounts for the 'bulk' contribution to the spectra, the NiO_5 pyramidal cluster represents the 'surface' contribution, and the connection between the clusters allows for non-local fluctuations. The Hamiltonian of this model is:

$$\begin{aligned}\hat{H} = &\sum_{i,m,\sigma} \varepsilon^d_{i,m,\sigma} \hat{d}^\dagger_{i,m,\sigma} \hat{d}_{i,m,\sigma} + \sum_{i,m,\sigma} \varepsilon^p_{i,m,\sigma} \hat{p}^\dagger_{i,m,\sigma} \hat{p}_{i,m,\sigma} \\ &+ \sum_{i,j,m,\sigma} T_{i,m} (\hat{d}^\dagger_{i,m,\sigma} \hat{p}_{j,m,\sigma} + H.c.) \\ &+ \sum_{i,m,n,\sigma\sigma} U_{m,n} \hat{d}^\dagger_{i,m,\sigma} \hat{d}_{i,m,\sigma} \hat{d}^\dagger_{i,n,\sigma}, \hat{d}_{i,n,\sigma} + \hat{H}_{mult} \end{aligned} \quad (1)$$

where $\hat{d}^\dagger_{i,m,\sigma}(\hat{p}_{i,m,\sigma})$ creates (annihilates) a d (p) electron with energy $\varepsilon^d_{i,m,\sigma}(\varepsilon^p_{i,m,\sigma})$. The indices i,j denote the cluster site ('bulk' or 'surface'), m,n represent the different orbitals, and σ denotes spin.

The main parameters of this model are the d–d Coulomb repulsion U, the core hole potential $Q = 1.2\,U$, the charge transfer energy $\Delta = \varepsilon_d - \varepsilon_p + U$, and the p–d hybridization T_i, [18]. In the 'bulk' cluster, the hybridization is given by T_σ (e_g symmetry). In the 'surface' cluster, the hybridization is given by $T_{basal} = T_\sigma$ (for the $x^2 - y^2$ level) and $T_{apical} = 2/3\ T_\sigma$ (for the z^2 level), where the reduction of T_{apical} is due to the absence of one apical oxygen.[8] The cluster is solved within the configuration interaction method. The ground state is expanded in the (bulk:surface) $3d^8$:$3d^8$, $3d^9\underline{L}$:$3d^8$, $3d^8$:$3d^9\underline{L}$, $3d^7$:$3d^9$, $3d^7$:$3d^{10}\underline{L}$, $3d^9$:$3d^7$, $3d^{10}\underline{L}$:$3d^7$, etc. configurations, where $\underline{L}$ denotes a hole in the O $2p$ band. The initial energy position of these configurations is presented in Table 1. They are further split into different multiplets ($\hat{H}_{mult}$), which are given in terms of the Raccah parameters B and C and the crystal field parameter $10Dq$. The values of all cluster model parameters are shown in Table 2. The corresponding core level state is obtained from the ground state by creating a core hole. The Hamiltonian is solved by exact diagonalization and the core level spectral weight $A(\omega)$ is calculated using the sudden approximation:

$$A(\omega) = \sum_i |\langle \psi^{CL}_i | \hat{O} | \psi^N_0 \rangle|^2 \delta(\omega - E^{CL}_i + E^N_0) \quad (2)$$

where $E^N_0(\psi^N_0)$ is the ground state energy (wavefunction) and $E^{CL}_i(\psi^{CL}_i)$ is the ith core level energy (wavefunction). The transition operator $\hat{O}$ is given by:

$$\hat{O} = g(\lambda)\hat{c}_b + (1 - g(\lambda))\hat{c}_s \quad (3)$$

where $\hat{c}_b(\hat{c}_s)$ annihilates a core electron in the 'bulk' ('surface') cluster, and $g(\lambda)$ is a weight function, which depends on the photoelectron kinetic energy, or its mean free path λ.

Table 1
Cluster model ground state configurations and energy positions.

Configuration	Energy position
$3d^8$:$3d^8$	0
$3d^9\underline{L}$:$3d^8$; $3d^8$:$3d^9\underline{L}$	Δ
$3d^{10}\underline{L}^2$:$3d^8$; $3d^8$:$3d^{10}\underline{L}^2$	$2\Delta + U$
$3d^9\underline{L}$:$3d^9\underline{L}$	2Δ
$3d^{10}\underline{L}^2$:$3d^9\underline{L}$; $3d^9\underline{L}$:$3d^{10}\underline{L}^2$	$3\Delta + U$
$3d^{10}\underline{L}^2$:$3d^{10}\underline{L}^2$	$4\Delta + 2U$
$3d^7$:$3d^9$; $3d^9$:$3d^7$	U
$3d^7$:$3d^{10}\underline{L}$; $3d^{10}\underline{L}$:$3d^7$	$U + \Delta$

Table 2
Cluster model parameters (all values in eV).

Parameter	Value
Δ	4.0
U	7.5
T_σ	1.5
B	0.13
C	0.58
10Dq	1.0

4. Results and discussion

4.1. Calculated core-level spectra

Figure 2 shows the calculated core-level spectra for the NiO_6 (bulk), NiO_5 (surface), and NiO_6:NiO_5 (surface + non-local) clusters. The discrete transitions were convoluted with a gaussian function. The labels are related to the main contribution of each final state configuration.

The lower panel of Figure 2 shows the core-level spectra calculated with a single octahedral NiO_6 cluster. This well known spectrum presents two main components: a main peak (green) at about 854.6 eV, and a charge transfer (CT) satellite (cyan) at around 861.9 eV. The main peak region has one final state, which is mainly formed by the $\underline{c}3d^9\underline{L}$ configuration, whereas the CT satellite region has two final states, which are mostly due to the $\underline{c}3d^{10}\underline{L}^2$ and $\underline{c}3d^8$ configurations.

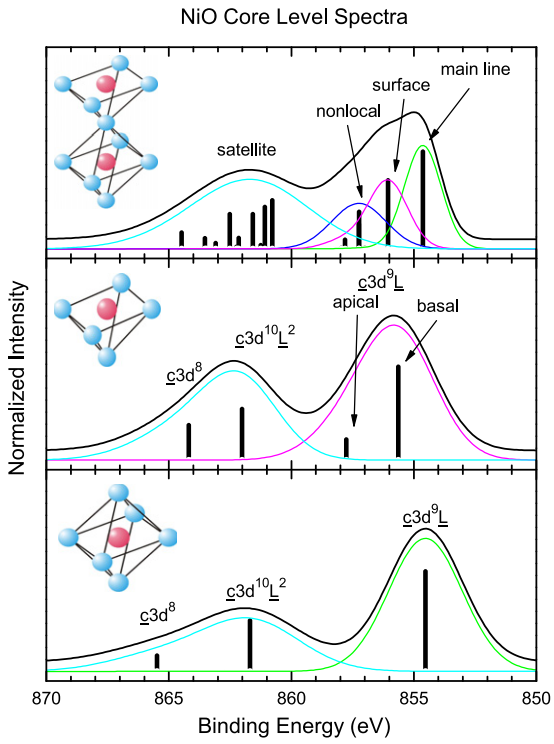

Figure 2. Calculated core-level spectra for the NiO_6 (bulk), NiO_5 (surface), and NiO_6:NiO_5 (bulk + surface + non-local) clusters. The discrete transitions were convoluted with a Gaussian function. The labels are related to the main contribution of each final state configuration.

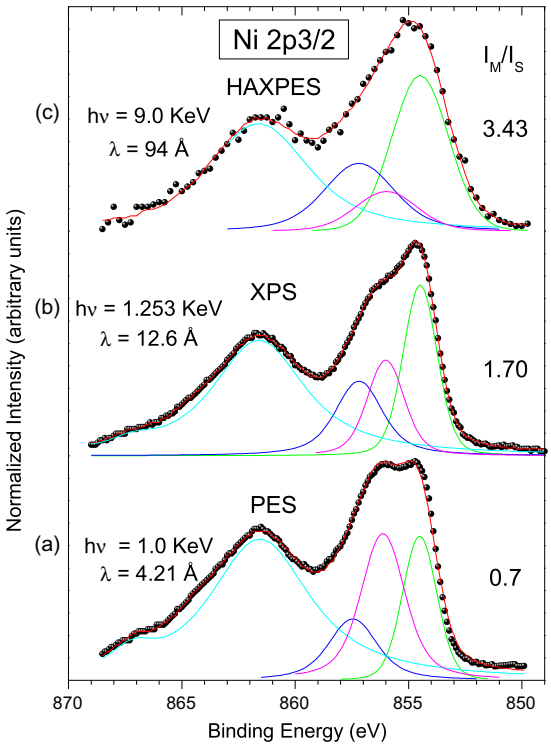

Figure 3. Experimental Ni $2p_{3/2}$ photoemission spectra of NiO measured at (a) 9.0 keV, (b) 1.486 keV and (c) 1.0 keV. The figure also shows the main line to surface intensity ratio (I_M/I_S) values obtained from the fittings and the inelastic mean free path λ (IMFP) for each photon energy.

The middle panel of Figure 2 shows the core-level spectra calculated with a single pyramidal NiO_5 cluster. The main peak (magenta) now appears at around 855.8 eV, whereas the satellite (cyan) is at about 862.2 eV. In this case, the $\underline{c}3d^9\underline{L}$ final state configuration is split into two different contributions (basal and apical), and the energy separation between the main line and the satellite is reduced by about 1.0 eV. These effects are attributed to the changes in the effective *p–d* hybridization due to the absence of an apical oxygen.

The top panel of Figure 2 shows the core-level spectra calculated with the NiO_6:NiO_5 cluster. The spectra now has three main components: a main peak at about 854.9 eV, a shoulder at around 861.6 eV, and a CT satellite at about −1.5 eV. Interestingly, the spectrum is not just the combination of the NiO_6 and NiO_5 cluster results, but a third component appears in the main peak/shoulder energy region. The main line (green) structure is mainly related to a configuration screened by an oxygen electron at the 'bulk' cluster ($\underline{c}3d^9\underline{L}$:$3d^8$). The surface (magenta) feature is mostly attributed to a configuration screened by an oxygen electron at the 'surface' cluster ($3d^8$:$\underline{c}3d^9\underline{L}$). Finally, the additional non-local contribution (blue) is mainly related to a configuration screened by an electron coming from the neighboring Ni ion ($\underline{c}3d^9$:$3d^7$ and $3d^7$:$\underline{c}3d^9$).

4.2. Ni $2p_{3/2}$, photoemission spectra

Figure 3 shows the Ni $2p_{3/2}$ photoemission spectra of NiO measured at (a) 9.0 keV, (b) 1.486 keV and (c) 1.0 keV. At first sight, the three experimental spectra are similar and present the same structures, although the energy resolution of the spectrum taken at 9 keV is worse.

The main difference between these spectra is that the relative intensity of the shoulder decreases with the photon energy. The spectra in Figure 3 were fitted using four different Gaussian functions accounting for: the main line (854.5 eV), the surface component (856.1 eV), the non-local component (857.3 eV), and the charge-transfer satellite (861.4 eV). All fittings have been performed by using the NewFit software from the Freie Universitat Berlin [19]. This software allows the fitting of multiple curves with fixed or variable parameters (position, width, intensity, etc.). The experimental resolution is included as other independent parameter. All fittings shown in Figure 3 have been performed by using the same fixed parameters for the main line peak and the non-local peak. Only the surface peak has been kept free in order to evaluate its intensity, energy position and width. The broadening of the Gaussian function was also adapted to take into account the experimental resolution. It is seen that the fittings are in very good agreement with the experimental results, see Figure 3.

The results show that the intensity of the surface component decreases with the photon energy. In turn, this diminution is related to the increase of the inelastic mean free path λ (IMFP) of the photoelectrons. In fact, the main line to surface intensity ratio (I_M/I_S) values obtained from the fittings in Figure 3 are in agreement with the trend of the λ values obtained from the Tanuma, Penn and Powell formula [20]. We have to note that recently, this formula has been validated for kinetic energies up to 30 keV, thus being suitable for the calculations of the IMFP of the spectrum taken at 9 keV [21].

4.3. Comparison with the experimental spectra

Figure 4 compares the experimental Ni $2p_{3/2}$ photoemission spectra of NiO with the cluster model calculations. The 'bulk' and 'surface' contributions to the spectra were weighted to give the best agreement with the experiment. The 'bulk' spectrum contributes with the main line, the non-local, and the satellite features, whereas the 'surface' spectrum includes the surface, the non-local, and the satellite peaks. The resulting surface contribution was 55%,

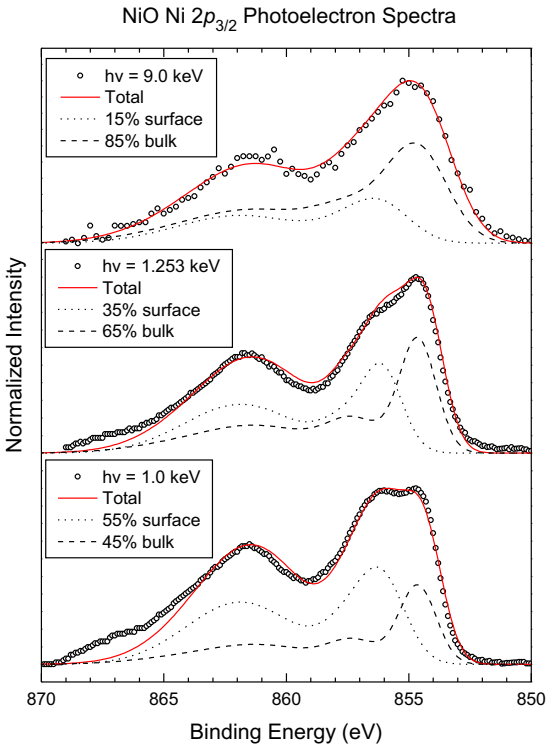

Figure 4. Experimental Ni $2p_{3/2}$ photoemission spectra of NiO compared with the cluster model calculations. The 'bulk' and 'surface' contributions to the spectra were weighted to give the best agreement with the experiment.

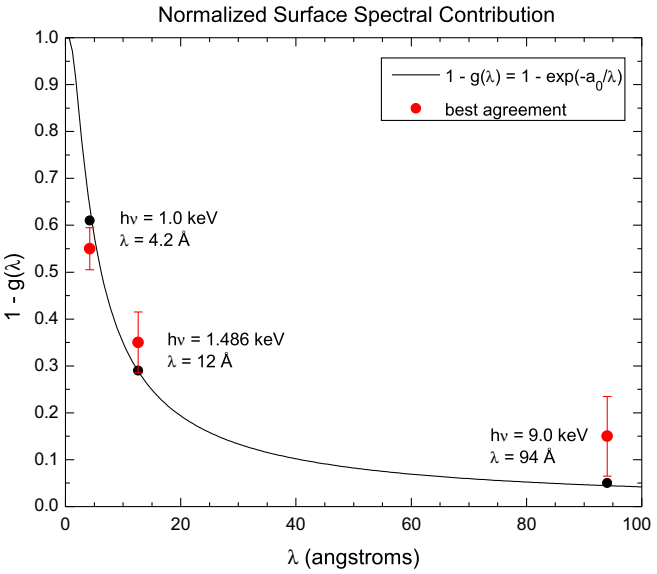

Figure 5. Weight of the surface contribution to the spectra as a function of the photoelectron mean free path λ. The values, for each photon energy, for the assumed model of $1 - g(\lambda)$ appear in black. The values used in our cluster model to fit the experimental spectra appear in red. (For interpretation of the references to colour in this figure legend, the reader is referred to the web version of this article.)

35% and 15% for the 1.0 keV, 1.486 keV and 9.0 keV spectra, respectively. The decrease of the surface component is again related to the increase of the corresponding IMFP. It is worth noting that the relative non-local contribution does not change much for any bulk/surface ratio.

4.4. Bulk versus surface contribution

We assume that the total spectrum is a weighted sum between the 'bulk' and 'surface' spectra:

$$A_{\text{total}}(\lambda) = g(\lambda)A_{\text{bulk}} + (1 - g(\lambda))A_{\text{surface}} \quad (4)$$

The weight function $g(\lambda)$ is approximated by:

$$g(\lambda) = e^{-\frac{a_0}{\lambda}} \quad (5)$$

where a_0 is the NiO lattice parameter, and λ is the photoelectron mean free path.

Figure 5 shows the weight of the surface contribution as a function of the photoelectron mean free path λ. The black line corresponds to the weight function $1 - g(\lambda)$ for the lattice parameter of the NiO samples (a_0 = 4.1769 Å). When λ is small, the photoelectrons originate mainly from the surface region and the surface contribution is larger. On the other hand, if λ is large, the photoelectrons come from deeper regions in the sample and the surface contribution is smaller.

The black dots in Figure 5 correspond to the values of $1 - g(\lambda)$ for the different λ obtained in Figure 3. The 'surface' contribution to the total spectral would be about 60%, 30% and 5%, respectively. On the other hand, the red dots in Figure 5 are the values of $1 - g(\lambda)$ used to weight the calculated core-level spectra in Figure 4. The 'surface' contribution in this case is around 55%, 35% and 15%, respectively. This concordance supports the idea that the changes in the spectra are related to the decrease of the surface component.

According to this picture, the spectrum of a NiO monolayer grown on MgO (100) [11] would be dominated by the surface component, whereas the spectrum of a Ni impurity diluted in MgO ($Ni_{0.1}Mg_{0.9}O$) [10] would be given by the bulk component alone. Finally, the increase of the shoulder intensity found in Ref. [7] when calculating the Ni $2p$ spectra for a Ni_6O_{30} cluster with respect to that for a Ni_7O_{36} cluster is perfectly consistent with our model, in which the removal of a NiO_6 cluster from the original one gives rise to the lack of the apical oxygen, thus enhancing the surface effect.

In our previous work [8], we studied the relative surface contribution by reducing the take-off angle. In this work, we study the relative bulk contribution using Hard X-ray Photoemission Spectroscopy (HAXPES). Therefore, this work extends and complements our previous results, confirming our conclusions. On the other hand, our previous results were analyzed using a separated pyramidal–octahedral cluster. Whereas the present results are analyzed using a combined pyramidal–octahedral cluster, which allows to describe not only the surface and the bulk contribution, but also the non-local contribution. This shows that this manuscript presents indeed new experimental results as well as an improved theoretical description.

Taguchi et al. [9] used non-local charge fluctuations from Zhang-Rice singlets, which are well suited to study the lowest energy states of doped compounds. The corresponding charge transfer energy Δ^* is relatively small (~1.5 eV), so the lowest energy excitation contains mainly ZRS character. On the other hand, we are using non-local charge fluctuations of the Mott–Hubbard type, which are better suited to study the electronic structure of undoped systems. The corresponding Mott–Hubbard energy in this case is relatively large (~7.5 eV), which produces a higher energy excitation, and the lowest energy excitation comes from a charge transfer from the O $2p$ states. Our approach is consistent with the work of Van Veenendaal et al. [7], which should be more appropriate for the photoemission spectra of undoped NiO.

5. Summary and conclusions

We studied the Ni 2*p* core-level spectra by using cluster model calculations of a NiO_6 cluster in contact to a NiO_5 cluster. This cluster symmetry enables the observation of bulk, surface, and non-local effects. The calculated spectrum has four main components: the main line (screening from oxygen atoms from a NiO_6 bulk cluster), surface component (screening from oxygen atoms from a NiO_5 surface cluster), non-local component (screening from the second neighbors in both symmetries), and charge-transfer satellite. The calculations are in agreement with the experimental spectra taken with both soft and hard X-rays. The decrease of the shoulder is attributed to a diminution of the surface component, which, in turn, is related to the increase of λ with photon energy. Our model opens a new perspective in analyzing the photoemission Ni 2p spectra of NiO nanostructures where the surface-to-volume ratio is significantly increased.

Acknowledgments

This work has been financially supported by the Spanish Ministerio de Ciencia e Innovación (MICINN) through project CONSOLIDER-INGENIO FUNCOAT Ref. CSD2008-00023 and project MAT2007-66719-C03-03, the Comunidad de Madrid contract NANOBIOMAGNET, Ref. S2009/MAT-1726, and the European Union through the R II 3.CT-2004-506008 contract. This work was also supported by Conselho Nacional de Desenvolvimento Científico e Tecnológico (CNPq). We thank the staff of BM25-SpLine at ESRF and BESSY II for technical support.

References

[1] A. Fujimori, F. Minami, S. Sugano, Phys. Rev. B 29 (1984) 5225.
[2] G.A. Sawatzky, J.W. Allen, Phys. Rev. Lett. 53 (1984) 2339.
[3] S. Hüfner, Solid State Commun. 52 (1984) 793.
[4] M.J. Tomellini, J. Electron Spectrosc. Relat. Phenom. 58 (1992) 75.
[5] A.F. Carley, S.D. Jackson, J.N. O'Shea, M.W. Roberts, Surf. Sci. 440 (1999) L868.
[6] M. Oku, H. Tokuda, K. Hirokawa, J. Electron Spectrosc. Relat. Phenom. 53 (1991) 201.
[7] M.A. Van Veenendaal, G.A. Sawatzky, Phys. Rev. Lett. 70 (1993) 2459.
[8] L. Soriano, I. Preda, A. Gutiérrez, S. Palacín, M. Abbate, A. Vollmer, Phys. Rev. B 75 (2007) 233417.
[9] M. Taguchi et al., Phys. Rev. Lett. 100 (2008) 206401.
[10] K. Okada, A. Kotani, J. Phys. Soc. Jpn. 60 (1991) 772.
[11] D. Alders, F.C. Voogt, T. Hibma, G.A. Sawatzky, Phys. Rev. B 54 (1996) 7716.
[12] L. Sangaletti, L.E. Depero, F. Parmigiani, Solid State Commun. 103 (1997) 421.
[13] L. Soriano, A. Gutiérrez, I. Preda, S. Palacín, J.M. Sanz, Phys. Rev. B 74 (2006) 193402.
[14] I. Preda, L. Soriano, L. Alvarez, J. Méndez, F. Yubero, A. Gutiérrez, J.M. Sanz, Surf. Interface Anal. 42 (2010) 869.
[15] G.R. Castro, J. Synchrotron. Rad. 5 (1998) 657.
[16] J. Rubio-Zuazo, M. Escher, M. Merkel, G.R. Castro, J. Phys.: Conf. Ser. 100 (2008) 072032.
[17] J. Rubio-Zuazo, G.R. Castro, Nucl. Instrum. Method. Phys. Res. A 547 (2005) 64.
[18] A.E. Bocquet et al., Phys. Rev. B 53 (1996) 1161.
[19] NewFit software, copyright held by Ch. Schüßler-Langeheine and the Freie Universität, Berlin.
[20] S. Tanuma, C.J. Powell, D.R. Penn, Surf. Interface Anal. 21 (1993) 165.
[21] Published on-line: doi:10.1002/sia.3522.